Rydberg-atom formation in strongly correlated ultracold plasmas

G. Bannasch* and T. Pohl

Max Planck Institute for the Physics of Complex Systems, Nöthnitzer Strasse 38, D-01187 Dresden, Germany

(Received 29 September 2011; published 11 November 2011)

In plasmas at very low temperatures, the formation of neutral atoms is dominated by collisional three-body recombination, owing to the strong $\sim T^{-9/2}$ scaling of the corresponding recombination rate with the electron temperature T. While this law is well established at high temperatures, the unphysical divergence as $T \to 0$ clearly suggests a breakdown in the low-temperature regime. Here, we present a combined molecular dynamics Monte Carlo study of electron-ion recombination over a wide range of temperatures and densities. Our results reproduce the known behavior of the recombination rate at high temperatures, but reveal significant deviations with decreasing temperature. We discuss the fate of the kinetic bottleneck and resolve the divergence problem as the plasma enters the ultracold, strongly coupled domain.

DOI: 10.1103/PhysRevA.84.052710 PACS number(s): 34.80.Lx, 34.80.Dp, 52.27.Gr, 52.65.Yy

I. INTRODUCTION

Since the first creation of ultracold plasmas (UCPs) via photoionization of laser-cooled atoms [1] or cold molecules [2], these systems have proved to provide a well-suited platform for studying a range of plasma physics phenomena, such as collective waves [3–9], plasma expansion into vacuum [10–17], plasma instabilities [18,19] and recombination of neutral atoms [20–24]. Besides opening up a new parameter regime [25–27] as well as promising applications for nanotechnology [28–31], UCPs offer a rare opportunity to study strongly correlated plasmas [32–35] in the laboratory.

The degree of correlations is characterized by the Coulomb coupling parameter $\Gamma = \frac{e^2}{a\,k_B T}$, where e is the electron charge, k_B is the Boltzmann constant, and $a = (\frac{4}{3}\pi\rho)^{-\frac{1}{3}}$ is the Wigner-Seitz radius for a plasma of density ρ. When the average potential energy $\sim e^2/a$ of the charges exceeds their thermal energy $\sim k_B T$, i.e., when $\Gamma > 1$, the plasma is termed strongly coupled. Strong coupling phenomena studied in UCPs include disorder-induced heating [36–41] accompanied by kinetic energy oscillations [42–44] as well as liquidlike [45] and crystalline [46–48] behavior of the ionic plasma component. In experiments [25–27] UCPs typically are created at densities of $\rho \approx 10^8$–10^{10} cm^{-3}, and with initial kinetic energies corresponding to ion temperatures of $T_i \approx 1$–10^3 μK and electron temperatures of $T \approx 1$–1000 K. The role of quantum effects in a plasma can be characterized by the Brueckner parameter $r_s = (\frac{4}{3}\pi\rho)^{-1/3}\frac{e^2 m}{\hbar^2}$ (m is the particle mass) [32], which becomes important as $r_s \lesssim 1$. Despite their ultralow temperatures, the very small density implies that $r_s > 5 \times 10^4$, such that currently realized UCPs behave entirely classically.

However, in contrast to dense strongly coupled plasmas, UCPs have a rather short life time on the order of several 10^2 μs. The dominant decay mechanism is collisional recombination leading to the formation of highly excited neutral Rydberg atoms. The corresponding rate constant $\nu \sim T^{-9/2}$ [49] has a strong dependence on the electron temperature T and can, hence, assume large values in UCPs. In the underlying three-body recombination (TBR) process two electrons collide in the vicinity of an ion to form a weakly bound Rydberg atom, where the remaining electron carries away the corresponding excess energy. Subsequent collisions of the formed Rydberg atom with free electrons can further deexcite the atom, and the released binding energy leads to an increase of the free-electron temperature T in the course of the plasma evolution [11,12,14,21,50].

The strong temperature dependence of the recombination rate can be readily established from simple scaling arguments. The collision frequency of an electron with average velocity $\bar{v} \sim \sqrt{T}$ is given by $\nu_c = \bar{v} b^2 \rho_e$, where ρ_e is the electron density and $b \sim T^{-1}$ is the characteristic distance of closest approach. Since the probability of finding another electron within a distance b of the colliding pair is $b^3\rho_e$, one obtains a TBR rate of $\nu \sim \nu_c\, b^3 \rho_e \sim \rho_e^2 T^{-\frac{9}{2}}$. In their seminal paper [49] Mansbach and Keck presented a detailed study of TBR in ideal plasmas. Performing classical trajectory Monte Carlo (CTMC) simulations of isolated three-body collisions and using rate equations, they confirmed the $T^{-\frac{9}{2}}$ scaling of the recombination rate and calculated the corresponding proportionality constant. Subsequent studies based on CTMC calculations or rate equations [23,51–53] have since confirmed the strong temperature dependence, which was found to be in good agreement with experiments in hot and cold ($T > 10\,000$ K) plasmas [51,52,54] as well as with measurements on UCPs with moderate coupling strength ($\Gamma \lesssim 0.2$) [22,23].

On the other hand, the strong temperature dependence of the TBR rate ultimately suggests unphysically fast recombination in the ultracold regime. It was one of the major motivations of early UCP experiments [1,20] to shed light on this apparent divergence problem of the recombination rate. The conflicting time scales and the role of particle correlations become particularly evident by transforming to dimensionless units, employing the electronic plasma frequency $\omega_p = \sqrt{4\pi e^2 \rho_e / m}$ such that

$$\nu \sim \rho_e^2\, T^{-9/2} \sim \omega_p\, \Gamma^{9/2}. \tag{1}$$

Consequently, for $\Gamma \gtrsim 1$ the recombination rate ν would become comparable to or larger than the plasma frequency ω_p, whose inverse determines the typical time scale of electronic motion in the plasma. The unphysical crossover of time

*bannasch@pks.mpg.de

scales at $\Gamma \gtrsim 1$ indicates a breakdown of the conventional recombination theory in terms of three-body collisions and suggests a modification of the recombination rate in the strongly coupled regime.

This fundamental problem has been addressed theoretically in a number of previous articles [53,55–63]. In [55–59] strong coupling in a dense plasma, where quantum effects become important, was considered and an enhancement of the recombination rate coefficient (and ionization rate coefficient) due to correlation-induced continuum lowering was found. On the other hand, studies of recombination in classical plasmas based on analytical estimates or numerical calculations [60,61,63,64] found a suppression of recombination in the moderately to strongly coupled regime, but the proposed modifications of the recombination rate yield different and contradictory results for the temperature scaling, such that the question of Rydberg-atom formation in correlated plasmas still remains an unsettled issue.

In this article, we investigate the classical recombination of a single ion immersed in a strongly coupled electron plasma without employing any additional approximation. Our calculations are based on Monte Carlo (MC) sampling of classical molecular dynamics (MD) simulations that provide a natural extension of previous three-body CTMC calculations [23,49] to account for strong electron-electron correlations and many-body interactions. Our results quantitatively reproduce the known behavior of the recombination rate [23] for $\Gamma \ll 1$ and are consistent with the results of Kuzmin and O'Neil [65] for the particular value of $\Gamma = 0.6$ studied in that work. We further discuss simulations of two-component plasmas for various initial configurations and temperatures, which demonstrate strong disorder-induced electron heating to $\Gamma \sim 0.5$. This conclusively excludes the possibility of a metastable plasma state with orders-of-magnitude suppression of recombination as suggested in [63,64]. Nevertheless, strong coupling effects on the recombination rate are found to have observable consequences during the short-time evolution of UCPs.

The article is organized as follows. Details of the plasma model as well as the numerical approach are given in Sec. II, where we also review the rate equation description of TBR based on CTMC collision rates. In Sec. III we discuss the obtained behavior of the bottleneck binding energy as a function of Γ, allowing us to calculate the recombination rate, presented in Sec. IV. Finally, Sec. V provides simulation results for two-component neutral plasmas and a discussion of competing heating effects and their consequences for the recombination dynamics.

II. NUMERICAL APPROACHES

To study Rydberg-atom formation at a constant temperature and to isolate the recombination from other collision processes (see Sec. V) we first consider the recombination dynamics of a single ion placed inside an electronic one-component plasma (OCP), consisting of N electrons and a homogeneous neutralizing positively charged background. While this model can only provide a simplified description of a neutral two-component system (see Sec. V) it resembles the situation of antihydrogen production experiments carried out at CERN [66–68]. Here highly excited antihydrogen Rydberg atoms are formed via successive transits of antiprotons through an ultracold positron plasma. In these experiments atoms are formed predominantly via collisional recombination, which is, however, considerably modified by the presence of applied strong magnetic fields, as has been extensively studied via CTMC calculations [69–74].

Our simulations proceed in three steps. First, we equilibrate the electron OCP to a predefined temperature Γ^{-1}. Subsequently, we place a neutral atom at the center of the cubic simulation box, consisting of an ion and an electron at the origin with the electron having an excess kinetic energy of $\frac{3}{2\Gamma}\frac{e^2}{a}$. This procedure ensures that the total potential energy is not affected by the introduction of the additional ion and at the same time gives a good description of atomic single-photon ionization used to produce UCPs [1]. Following the escape of the "photo-electron" we monitor the evolution of the surrounding plasma electrons.

A. Molecular dynamics simulation

The computationally most demanding part of the simulation is the evaluation of the mutual interactions between the N plasma electrons. Due to the $O(N^2)$ of the corresponding numerical effort and the necessity to implement periodic boundary conditions (PBC), a straightforward force calculation would be prohibitively demanding in view of the accuracy and ensemble size required for the present study.

Both of these problems can be efficiently resolved by the fast multipole method (FMM) [75] which permits force calculations for large particle numbers with a complexity of $O(N)$. The FMM algorithm divides the simulation volume into a hierarchy of cubic subcells, and determines multipole expansions for the charge distribution in each cell. The interaction of a certain particle with the particles in a distant cell can then be calculated much more efficiently and with a controllable error. Moreover, the FMM provides a natural implementation of PBC, as the periodic images of the simulation box can be treated as an upper extension of the hierarchy of cubic subcells [76]. The particular implementation of the FMM used in this work is described in [77,78]. As discussed below, our algorithm also requires us to calculate interactions among a small subgroup of particles. In this case, we perform a direct force summation and implement PBC via the standard Ewald summation [79,80].

To initiate the photo-electron at the central ion position we remove the singularity of the attractive electron-ion potential according to

$$V_{\mathrm{ion}}(r) = \begin{cases} -\frac{e^2}{r} & r > r_{\mathrm{c}}, \\ -\frac{3\,e^2}{2\,r_{\mathrm{c}}}\left(1 - \frac{r^2}{3r_{\mathrm{c}}^2}\right) & r \leqslant r_{\mathrm{c}}. \end{cases} \tag{2}$$

where the soft-core radius $r_{\mathrm{c}} = 10^{-2}a$ was chosen sufficiently small as to have no influence on the simulation results, as has been checked by varying the value of r_{c}.

Consequently, the magnitude of the electron-ion force is limited by $F^{\mathrm{ei}}_{\mathrm{max}} = e^2/r_{\mathrm{c}}^2$. Typically, $F^{\mathrm{ei}}_{\mathrm{max}}$ will be much larger than the characteristic force between the electrons $F^{\mathrm{ee}} \sim \Gamma^{-2}$, which induces two vastly disparate time scales of the electron motion: Far from the central ion, electrons

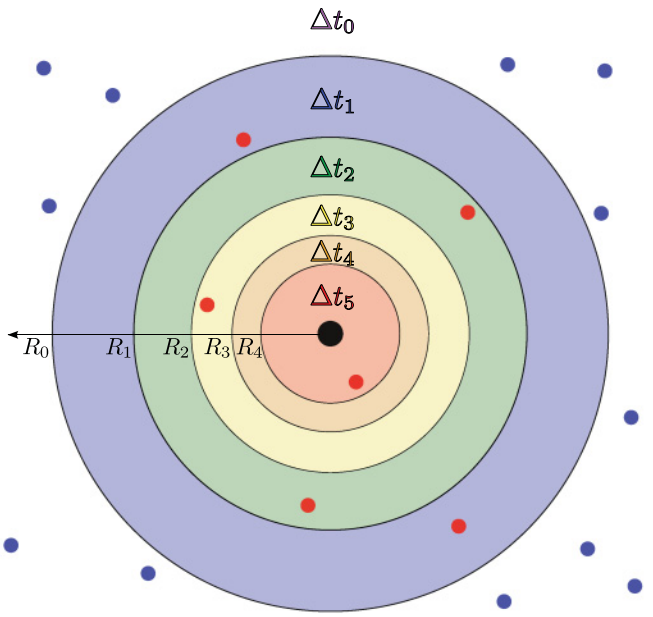

FIG. 1. (Color online) Two-dimensional projection of the center of the simulation cell with central ion (black dot) and the regions of different time steps. All electrons within the sphere $r < R_0$ (red dots) are propagated with the same reduced time step Δt_n which is determined by the smallest electron-ion separation $r_{\min}$, according to $R_n < r_{\min} < R_{n-1}$ (this example: $\Delta t_n = \Delta t_5$). Electrons with $r > R_0$ (blue dots) are propagated with the global time step Δt_0.

move comparatively slowly on a time scale $\sim\omega_p^{-1}$, while close to the ion, scattered and bound electrons undergo much faster dynamics. An efficient symplectic propagation of the electrons that exploits different system time scales can be realized by the so-called reversible reference system propagator algorithm (r-RESPA) [81,82]. In the present case, the principal idea is to evaluate the dynamics of distant electrons (blue dots in Fig. 1) with a fixed, coarse-grained time step, while the electron motion in the immediate ion vicinity is resolved with a smaller, dynamically adapted time step. This guarantees an accurate description of the recombination process while maintaining computational costs at a minimum.

Usually the r-RESPA split is based either on forces or on particles [82]. The two time scales discussed above call for a force-based r-RESPA split by separating terms involving electron-ion interactions from terms which involve electron-electron interactions. However, as the condition $F^{\rm ei}_{\max} \gg F^{\rm ee}$ holds only for those few electrons which are close to the ion, it is more efficient to additionally split the Hamiltonian based on particles, by separating terms involving electrons with positions $r_i < R_0 = a$ from terms involving more distant electrons with $r_i > R_0$, $i = 1, \ldots, N$. The total Hamiltonian $\mathcal{H}$, describing the dynamics of the N electrons with position $\mathbf{r}_i$ and momentum $\mathbf{p}_i$ is thus split according to

$$\mathcal{H} = K^f + K^s + V^f + V^s + E_{\rm BG}\,, \tag{3}$$

where

$$K^f = \sum_{\substack{i=0\\ r_i<R_0}}^{N} \frac{\mathbf{p}_i^2}{2m}, \quad V^f = \sum_{\substack{j>i\\ r_i,r_j<R_0}}^{N} \frac{e^2}{|\mathbf{r}_i - \mathbf{r}_j|} + \sum_{\substack{i=0\\ r_i<R_0}}^{N} V_{\rm ion}(r_i)$$

denote the kinetic energy and interactions of particles in the region of fast dynamics ($r < R_0$). Likewise, the remaining energies in the region of slow dynamics ($r > R_0$) are given by

$$\begin{aligned} K^s &= \sum_{\substack{i=0\\ r_i>R_0}}^{N} \frac{\mathbf{p}_i^2}{2m}, \\ V^s &= \sum_{j>i}^{N} \frac{e^2}{|\mathbf{r}_i - \mathbf{r}_j|} + \sum_{\mathbf{L}\neq\mathbf{0}} \sum_{i,j}^{N} \frac{e^2}{|\mathbf{r}_i - \mathbf{r}_j + \mathbf{L}|} \\ &\quad + \sum_{\mathbf{L}} \sum_{i=0}^{N} V_{\rm ion}(|\mathbf{r}_i + \mathbf{L}|) - V^f, \end{aligned} \tag{4}$$

and $E_{\rm BG}$ is the particle-background interaction energy. The sum $\sum_{\mathbf{L}}$ runs over all possible lattice vectors in the periodic lattice of image simulation boxes. Because of TBR collisions, which will take place in the region of fast dynamics, the electron-electron interaction among electrons in this region can become comparable to the ion-electron interaction and has thus been included in V^f.

The majority of electrons participate in the slow dynamics and are propagated with a fixed global time step Δt_0. The corresponding electron-electron forces including image charges are calculated within the FMM, while the electron-ion interaction is obtained by direct force summation combined with the Ewald summation to implement the PBC. Note that the forces arising from the image charges change only slowly and, hence, can be entirely accounted for in the slow dynamics [cf. Eq. (4)].

Each electron within the critical distance $R_0 = a$ participates in the fast dynamics. For appropriate time-step adaption we divide this spherical region into concentric shells of radii $R_n = 2^{-n/2} R_0$, $n = 1,2,\ldots$ (see Fig. 1). Once the smallest electron-ion distance falls below R_n the time step for all electrons within R_0 is decreased to $\Delta t_{n+1} = 2^{-(n+1)}\Delta t_0$ (see Fig. 1). For the electron propagation in the region of fast dynamics with the small time step Δt_n the interaction V^f is calculated via direct force summation and the Ewald potential [79,80,83–85]. To avoid periodic changes of the time step Δt_n, the time step is only decreased as long as there are electrons in the region $r < R_0$. Only when an electron leaves the region of fast dynamics is its propagation switched back to the global time step Δt_0 (see Fig. 2). We set $\Delta t_0 = 10^{-3}\,\omega_p^{-1}$, ensuring accurate propagation for both free and bound electrons. In fact, we achieve a very small maximum relative energy error in all simulations below 0.01%. We find that such a high accuracy is needed in order to obtain reliable converged results for the recombination rate.

Formally, our propagator for the fast electrons can be written as

$$S^f(\Delta t_n) = U_{V^f}\left(\frac{\Delta t_n}{2}\right) U_{K^f}(\Delta t_n) U_{V^f}\left(\frac{\Delta t_n}{2}\right), \tag{5}$$

where we have used the notation employing propagators $U_A(t) = e^{t\mathcal{D}_A}$ of differential operators $\mathcal{D}_A = \{\mathbf{q}, A\}$. Here, $\{\ldots\}$ denotes the Poisson bracket, $\mathbf{q} = (\mathbf{r_1}, \mathbf{r_2}, \ldots, \mathbf{r_N}; \mathbf{p_1}, \mathbf{p_2}, \ldots, \mathbf{p_N})$, and A stands for any of the

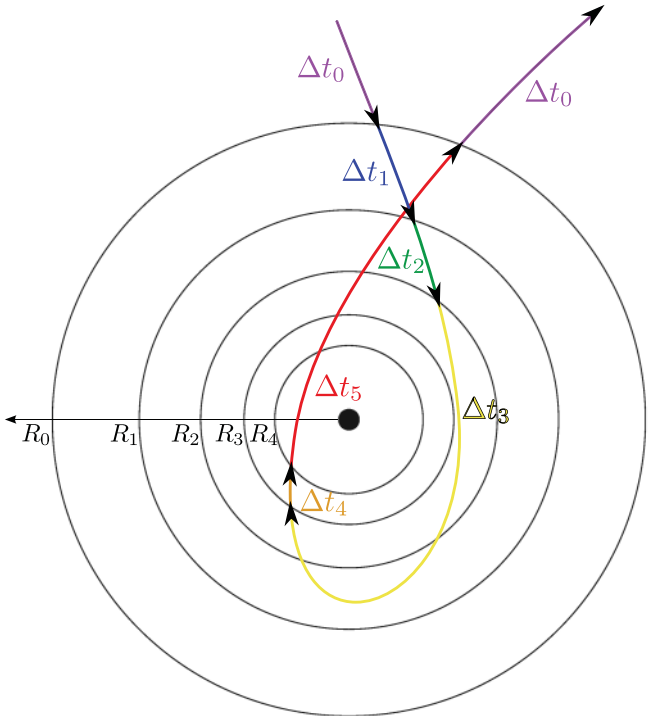

FIG. 2. (Color online) Schematics of the time step adaption as described in the text.

energy terms of the system Hamiltonian (3). The total system propagator is then given by

$$S(\Delta t_0) = U_{V^s}\left(\frac{\Delta t_0}{2}\right) U_{K^s}(\Delta t_0)\,[S^f(\Delta t_n)]^{2^n}\, U_{V^s}\left(\frac{\Delta t_0}{2}\right). \tag{6}$$

Besides the numerical challenges, a proper analysis of the MD data and in particular the identification and characterization of the formed classical bound states poses additional difficulties. The most straightforward way would be to monitor the electrons total energy E_i, i.e., the sum of the ith electron's kinetic energy and potential energy due to the ion, the remaining $N-1$ electrons, their periodic images and the positive homogeneous background, and declare an electron bound when $E_i < 0$. While this criterion makes sense for isolated atoms, in the present case many-body interactions and possibly strong electron-electron correlations lead to a lowered and fluctuating ionization threshold [86]. In fact, already for moderate coupling strength one finds that $E_i < 0$ for several electrons. Those electrons can be considered as weakly localized in slowly fluctuating potential wells formed by the correlated charges [87], but they are not bound by the ionic potential. Hence, once an electron becomes bound to the ion, its energy should drop significantly below the energies of free electrons. Therefore, we use the lowest electron energy $E_{\min}(t) = \min_{i\in N}[E_i(t)]$ as an initial criterion to select a possibly bound electron, whose index is denoted by $j_{\min}(t)$.

A typical example of such an minimal energy trajectory $E_{\min}(t)$ is shown in Fig. 3(a). As can be seen, $E_{\min}$ stays negative most of the time, and therefore provides only a necessary but not sufficient criterion for bound state assignment.

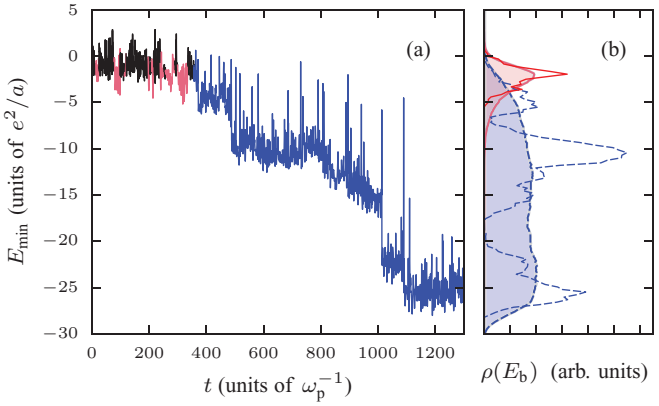

FIG. 3. (Color online) (a) Typical time evolution of the minimum electron energy $E_{\min}$. Black parts correspond to unbound electrons, red (light grey) parts to bound electrons that are subsequently ionized, blue (dark grey) parts to bound electrons that reach E_{sink} without ionization for $\phi_c = 4\pi$. (b) Corresponding energy densities ρ_{ion} (solid) and ρ_{rec} (dashed) of the example trajectory (lines) and as obtained from the ensemble average (shaded).

To detect stable electron-ion orbits we adopt the procedure proposed in [88] and integrate the rotation angle ϕ of the $j_{\min}$-th electron around the ion. If $j_{\min}$ changes its value, e.g., due to an exchange collision, integration starts again at zero. If the maximum rotation angle $\phi_{\max}(j_{\min})$ of the $j_{\min}$-th electron exceeds a critical angle ϕ_c the electron is considered to be bound. The binding energy $E_b(t)$ of a Rydberg atom corresponds to the parts in $E_{\min}(t)$ where $j_{\min}(t)$ fulfills this angular criterion:

$$E_b(t) = \begin{cases} 0 & \phi_{\max}(j_{\min}(t)) < \phi_c, \\ E_{\min}(t) & \phi_{\max}(j_{\min}(t)) \geqslant \phi_c, \end{cases} \tag{7}$$

i.e., $E_b(t) = 0$ in the absence of a bound state, as marked by the black segments in Fig. 3(a). The influence of the precise value of ϕ_c on the extracted recombination dynamics will be discussed below.

Following the initial capture, subsequent electron-atom collisions slightly (de)excite the formed atom, lead to reionization or occasionally drive the atom to significantly deeper binding energies. Such close collisions typically cause electron exchange [69] and are marked by sharp peaks in $E_b(t)$ [see Fig. 3(a)].

The simulation is stopped as soon as $E_b(t)$ reaches a certain energy sink E_{sink}. The energy sink was set to $E_{\text{sink}}/(e^2/a) = -20$ for $\Gamma \geqslant 1$ and to $E_{\text{sink}}/(e^2/a) = -50$ for $\Gamma < 1$ to ensure that the probability for a reionization vanishes well before the energy sink is reached (see Fig. 4) and therefore does not affect the final results for the determined recombination dynamics.

Physical quantities are extracted from averages over an ensemble of $\sim 10^3$ simulation runs per parameter set, produced in a Monte Carlo sampling over the initial positions and velocities of the electrons.

B. Rate equations

To make direct comparison to previous CTMC calculations, we also solved the corresponding rate equations for the recombination scenario discussed above. Here one calculates the

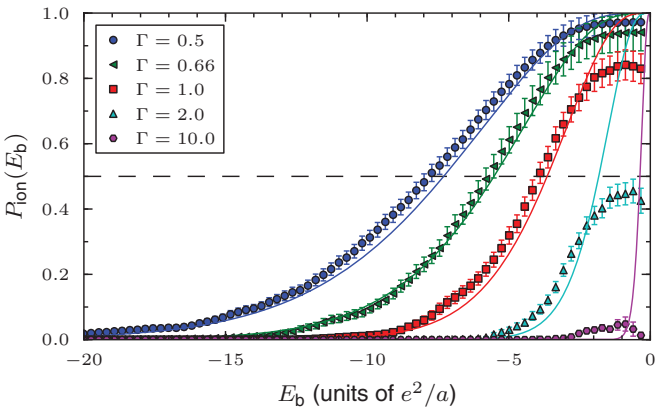

FIG. 4. (Color online) Ionization probability $P_{\rm ion}(E_{\rm b})$ for different Γ. Symbols correspond to MD data with $\phi_{\rm c} = 4\pi$. The lines show the ideal plasma prediction obtained by Eq. (16). The crossing with $P_{\rm ion} = \frac{1}{2}$ (dashed line) determines the location of the kinetic bottleneck $E_{\rm bn}$.

evolution of level population densities ρ_n of the recombining atom [51,62,89,90] according to

$$\frac{d\rho_n}{dt} = \rho_{\rm e}(t) \sum_{n' \neq n} [\rho_{n'}(t)\, R(n',n) - \rho_n(t) R(n,n')] + \rho_{\rm e}(t)^3 R_{\rm rec}(n) - \rho_{\rm e}(t)\, \rho_n(t) R_{\rm ion}(n), \quad (8a)$$

$$\frac{d\rho_{\rm e}}{dt} = \rho_{\rm e}(t) \sum_{n'} [\rho_{n'}(t) R_{\rm ion}(n') - \rho_{\rm e}(t)^2 R_{\rm rec}(n')]. \quad (8b)$$

We use the transition rates recently determined in [23] by CTMC calculations. The rate for excitation from the atomic level n to level $n' > n$ is given by

$$R(n,n') = k_0\, \epsilon_{n'}^{3/2}\, e^{\epsilon_{n'} - \epsilon_n} \left[\frac{22}{(\epsilon_n + 0.9)^{7/3}} + \frac{9/2}{\epsilon_n^{5/2}\, \Delta\epsilon^{4/3}} \right], \quad (9)$$

the rate for deexcitation from n to $n' < n$ is given by

$$R(n,n') = k_0\, \frac{\epsilon_n^{5/2}}{\epsilon_{n'}} \left[\frac{22}{(\epsilon_{n'} + 0.9)^{7/3}} + \frac{9/2}{\epsilon_{n'}^{5/2}\, \Delta\epsilon^{4/3}} \right], \quad (10)$$

the rate for recombination into an atomic level n is given by

$$R_{\rm rec}(n) = \frac{11\, \sqrt{\mathcal{R}/k_{\rm B}T}\, k_0\, n^2\, \Lambda^3}{\epsilon_n^{7/3} + 4.38\, \epsilon_n^{1.72} + 1.32\epsilon_n}, \quad (11)$$

and the rate for ionization of atoms in level n is

$$R_{\rm ion}(n) = \frac{11\, \sqrt{\mathcal{R}/k_{\rm B}T}\, k_0\, e^{-\epsilon_n}}{\epsilon_n^{7/3} + 4.38\, \epsilon_n^{1.72} + 1.32\epsilon_n}, \quad (12)$$

where $k_0 = e^4/(k_{\rm B}T\sqrt{m\,\mathcal{R}})$, $\epsilon_n = \mathcal{R}/(n^2\, k_{\rm B}T)$, $\Delta\epsilon = |\epsilon_n - \epsilon_{n'}|$, $\Lambda = \sqrt{h^2/(2\pi\, m\, k_{\rm B}T)}$ is the thermal de Broglie wavelength, $\mathcal{R}$ is the Rydberg constant, and h is Planck's constant.

III. KINETIC BOTTLENECK

Generally, the recombination rate ν is defined as the rate at which ground-state atoms are populated in the plasma [51,53,62,89]. While such deeply bound states defy a classical description, it was shown in [49] that this rate can also be determined from the downward energy flux through a kinetic bottleneck energy that divides weakly bound from stable atomic states. As the bottleneck typically lies in the classical region of binding energies this process can be described classically.

The concept of the kinetic bottleneck is readily understood from the following simple arguments. Depending on its binding energy $E_{\rm b}$, a bound electron has a certain probability $P_{\rm ion}(E_{\rm b})$ for collisional reionization and a probability to be successively driven to deeper binding energies until it eventually reaches the ground state without being reionized on its way. In our simulations the latter equals the probability $P_{\rm sink}(E_{\rm b}) = 1 - P_{\rm ion}(E_{\rm b})$ for reaching the energy sink at $E_{\rm sink}$, since $P_{\rm ion}(E_{\rm sink}) \approx 0$. The reionization probability decreases with deeper binding and ultimately falls below the recombination probability, such that the atomic states become more and more stable against ionizing electron-atom collisions. Hence, the kinetic bottleneck is defined as the energy $E_{\rm bn}$ at which recombination starts to dominate, i.e., the energy at which

$$P_{\rm ion}(E_{\rm b} = E_{\rm bn}) = P_{\rm sink}(E_{\rm b} = E_{\rm bn}) = \tfrac{1}{2}. \quad (13)$$

Three-body CTMC calculations predict a simple linear scaling of the bottleneck [49]

$$E_{\rm bn} \approx -3.83\, \Gamma^{-1}\, \frac{e^2}{a}. \quad (14)$$

As the bottleneck energy is crucial for determining the recombination rate, we first need to check the validity of this simple law in the strong coupling regime. In the MD simulations, $E_{\rm bn}$ can also be determined from Eq. (13), where $P_{\rm ion}(E_{\rm b})$ is calculated from the corresponding bound-state energy densities obtained from the above-described energy trajectories (see Fig. 3) according to

$$\varrho_{\rm tot}(\epsilon) = \left\langle \int_0^\tau \delta(E_{\rm b}(t) - \epsilon)\, {\rm d}t \right\rangle, \quad (15)$$

where τ is the simulation time of a single simulation run and $\langle \ldots \rangle$ denotes the average over the statistical ensemble. This total energy density can be split into two parts, $\varrho_{\rm tot}(E_{\rm b}) = \varrho_{\rm ion}(E_{\rm b}) + \varrho_{\rm rec}(E_{\rm b})$. $\varrho_{\rm ion}(E_{\rm b})$ contains only bound states that are subsequently ionized, while $\varrho_{\rm rec}(E_{\rm b})$ counts only energies of bound states that reach the energy sink without intermediate reionization [red and blue, respectively, in Fig. 3(b)]. The ionization probability $P_{\rm ion}(E_{\rm b})$ is then obtained from the ratio $P_{\rm ion}(E_{\rm b}) = \frac{\varrho_{\rm ion}(E_{\rm b})}{\varrho_{\rm tot}(E_{\rm b})}$, and shown in Fig. 4 for several values of the Coulomb coupling parameter Γ.

For ideal plasmas ($\Gamma \to 0$) and within the adiabatic treatment of Bates, Kingston, and McWhirter [89], the ionization probability $P_{\rm ion}(E_{\rm b} = -\mathcal{R}/n^2)$ can be directly obtained from the collision rate equations (9)–(12) [53,90]

$$P_{\rm ion}(E_{\rm b}) = \frac{R_{\rm ion}(n)}{A(n)} + \sum_{n' \neq 1,n} \frac{R(n,n')\, R_{\rm ion}(n')}{A(n)\, A(n')} + \cdots, \quad (16)$$

by summing over the probabilities of all possible pathways in energy space that connect an atomic level of binding energy $E_{\rm b} = -\mathcal{R}/n^2$ to the continuum, where $A(n) = \sum_{n' \neq n} R(n,n') + R_{\rm ion}(n)$ is the total rate for leaving level n. The first term in Eq. (16) represents the probability that the bound electron will be ionized directly from level n. The

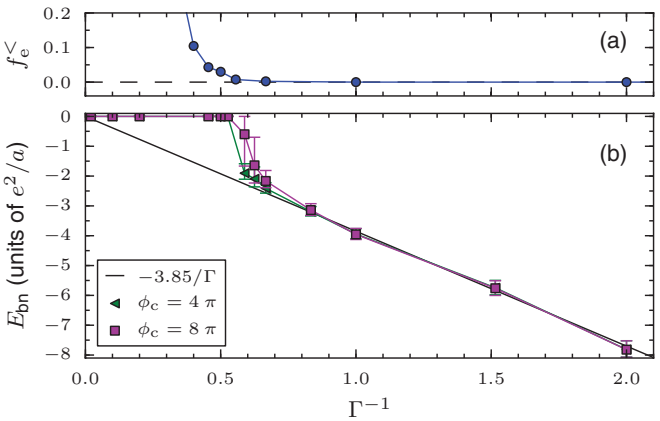

FIG. 5. (Color online) (a) Fraction $f_e^<$ of free electrons with energy $E < -4\,\Gamma^{-1}\,\frac{e^2}{a}$. (b) Bottleneck energy E_{bn} as a function of Γ for two different critical angles ϕ_c compared to the standard $-3.85\,\Gamma^{-1}\,\frac{e^2}{a}$ scaling (black line).

second term accounts for an intermediate step via a level n' from which subsequent ionization occurs, and so on.

The good agreement between our MD results and Eq. (16) in the regime of small to moderate Γ, shown in Fig. 4, attests to the accuracy of both approaches. In this regime the bottleneck energy can be straightforwardly determined according to Eq. (13) and corresponds to the intersections of P_{ion} and the horizontal dashed line at 0.5 in Fig. 4. At larger Γ values, however, the ionization probability is suppressed to $P_{ion}(E_b) < 0.5$ over the entire range of binding energies, such that the bottleneck energy vanishes.

The resulting temperature dependence of the bottleneck energy is shown in Fig. 5(b). For small coupling parameters the MD simulations predict a linear scaling, $E_{bn} = -3.85\,\Gamma^{-1}\frac{e^2}{a}$, in quantitative agreement with the three-body CTMC result, Eq. (14). However, for $\Gamma \gtrsim 2$, the bottleneck drops to zero. In contrast to the ideal plasma case, where electrons still have to overcome the kinetic bottleneck barrier before recombination, stable atoms are formed directly in the strongly coupled regime. The disappearance of the kinetic bottleneck can be traced back to correlation-induced continuum lowering, which around $\Gamma \approx 2$ leads to a merging of the ionization threshold and the bottleneck energy. To demonstrate this point, Fig. 5(a) shows the fraction $f_e^<$ of *free* plasma electrons with a total energy of $E_i < -4\,\Gamma^{-1}\,\frac{e^2}{a}$. The simulation results yield a steep increase of $f_e^<$ around $\Gamma \approx 2$, at which the bottleneck, thus, has to disappear, in agreement with Fig. 5(b). Consequently, the critical angle ϕ_c has almost no effect on the critical Γ at which the bottleneck energy drops to zero and can only slightly affect the value of E_{bn} for smaller Γ [see Fig. 5(b)].

IV. RECOMBINATION RATE

Having determined the location of the bottleneck we can now proceed to extract the recombination rate ν from our MD simulations. This is done in a straightforward manner by calculating the time-dependent recombination probability $P_{rec}(t)$, defined as the probability to observe a bound electron with binding energy $E_b(t) < E_{bn}$ at a time t. Figure 6

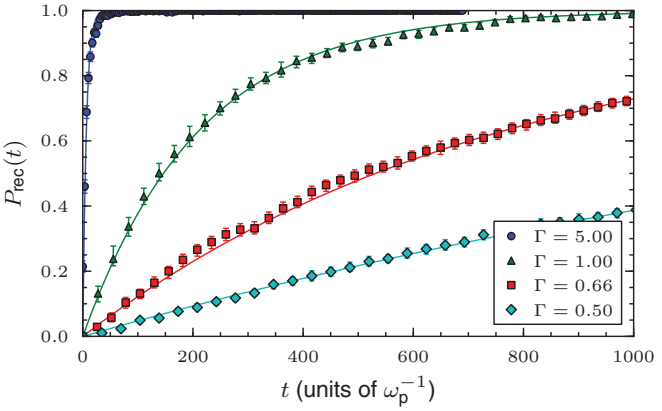

FIG. 6. (Color online) Recombination probability $P_{rec}(t)$ as a function of time for different coupling strengths Γ and $\phi_c = 4\pi$. The lines represent fits of Eq. (17) to the MD simulation result.

shows examples of the obtained $P_{rec}(t)$ for different coupling strengths and a critical angle $\phi_c = 4\pi$. The numerical data are well fitted by an exponential bound-state relaxation law of the form

$$P_{rec}(t) = 1 - e^{-\nu t}, \tag{17}$$

which permits us to extract the recombination rate ν.

Figure 7(b) shows the rate ν as a function of the inverse critical angle ϕ_c. One finds a linear dependence on $1/\phi_c$, whose slope tends to increase with increasing coupling strength. The fact that in the considered range of ϕ_c all simulation results perfectly lie on a line allows us to extrapolate to $1/\phi_c \to 0$, corresponding to stable atomic states.

For comparison with the weak coupling CTMC results, we also calculate the recombination rate [53]

$$\nu = \sum_n [1 - P_{ion}(-\mathcal{R}/n^2)]\, R_{rec}(n)\,, \tag{18}$$

as obtained from Eqs. (11) and (16). Figure 7(a) shows the extrapolated many-body MD (circles) and three-body CMTC

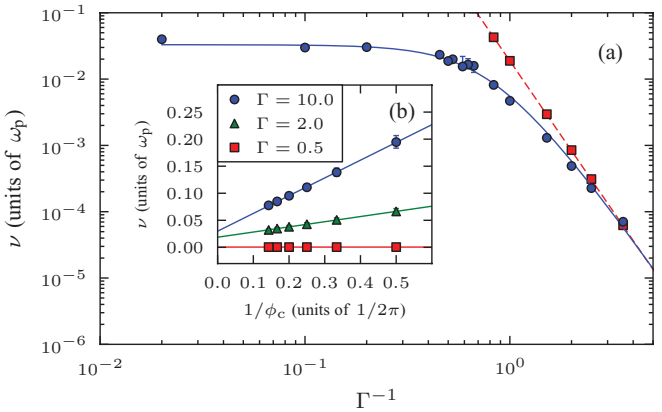

FIG. 7. (Color online) (a) Recombination rate ν as a function of inverse coupling strength Γ^{-1} calculated with MD simulations (circles) compared to the $\Gamma^{9/2}$ scaling obtained by Eq. (18) (squares). The dashed red line corresponds to Eq. (19), the solid blue line serves as guide to the eye. (b) Dependence of ν on inverse critical angle $1/\phi_c$ with fitted extrapolation (lines).

(squares) results for the recombination rate as a function of Γ^{-1}. In the weak coupling regime we find good quantitative agreement with the $T^{-9/2}$ scaling [23]

$$\nu \approx 0.019\,\omega_p\,\Gamma^{9/2}\,. \tag{19}$$

Notably, the MD results demonstrate the high accuracy of the rate equation description even for moderate coupling strength $\Gamma \lesssim 0.3$, corresponding to typical parameters in the long-time evolution of UCPs [11,50]. In the regime of strong Coulomb coupling, however, one finds a significant suppression of the recombination rate. Our result approaches a constant value of $\nu \approx 0.03\,\omega_p$ with increasing Γ, thereby resolving the apparent time-scale paradox described in Sec. I. At intermediate Γ values, our results are consistent with previous MD simulations of two-component plasmas [65]. These two-component simulations also predict a suppression by a factor of $\sim$2 for the particular value of $\Gamma = 0.6$ studied in [65], suggesting that the present OCP model should provide a good description of recombination in neutral plasmas. In this case, however, additional disorder-induced electron heating [37,38] limits the range of realizable Coulomb coupling parameters, as will be briefly discussed below.

V. TWO-COMPONENT PLASMA SIMULATIONS

The OCP calculations discussed above made it possible to initialize equilibrium plasmas with arbitrarily large values of Γ. Such calculations, however, do not account for electron heating due to the electron-ion interaction, which generally limits the electron coupling strength in UCP experiments. To study this effect as well as additional continuum lowering due to direct ion-ion interactions we also performed MD simulations of a two-component plasma (TCP) with N ions and N electrons in a cubic simulation cell with PBC. For these simulations, all interactions and the corresponding PBC are calculated within the FMM. We use a very small global time step $\Delta t = 10^{-5}\,\omega_p^{-1}$, ensuring an accurate treatment of even the lowest bound states observed in the simulations. In analogy to the previously described simulation scheme, the full plasma simulations start with N randomly distributed atoms which are photoionized at $t = 0$ as detailed in Sec. II A. The initial kinetic excess energy $E = \frac{3}{2\Gamma_0}\frac{e^2}{a}$ determines the initial effective coupling strength Γ_0, i.e., the scaled kinetic energy Γ_0^{-1}.

However, since this procedure creates a highly nonequilibrium plasma, it takes a finite time to establish a well-defined electron temperature. To characterize the corresponding initial relaxation we monitor the evolution of two different coupling parameters, defined through ith order momenta $\langle v^i \rangle$ of the free-electron velocity distribution

$$\Gamma_1 = 3/\langle v^2 \rangle, \tag{20a}$$

$$\Gamma_2 = \sqrt{6/(\langle v^4 \rangle - \langle v^2 \rangle^2)}. \tag{20b}$$

In local equilibrium, i.e., once the electrons have established a Maxwellian velocity distribution, $\Gamma_1 = \Gamma_2$. Indeed the simulation results in Figs. 8 and 9 show that both definitions of Γ approach each other on a timescale ω_p^{-1}, such that one can speak of an electron temperature for $t > \omega_p^{-1}$.

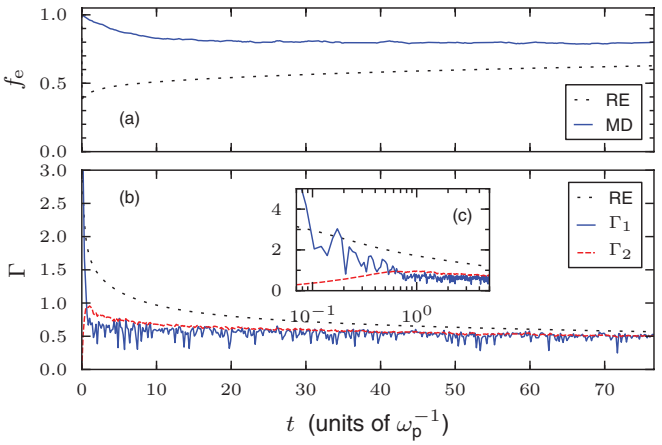

FIG. 8. (Color online) Evolution of the normalized free electron density f_e (a) and electronic coupling parameter Γ (b,c) calculated with MD simulations for $\phi_c = 4\pi$ and rate equation (RE) for an initial excess energy corresponding to the coupling strength of $\Gamma_0 = 50$.

On the same time scale, the electrons heat up due to disorder-induced heating [37,38]. As shown in Figs. 8 and 9, for both very large ($\Gamma_0 = 50$, Fig. 8) and moderate ($\Gamma_0 = 1$, Fig. 9) initial effective coupling strengths, the Coulomb coupling parameter relaxes to a value of $\Gamma \approx 0.5$ during the initial relaxation stage, which is a factor of $\sim$2 smaller than found in [38] but agrees with the findings of more recent MD simulations [91].

We have investigated the amount of initial heating for a range of initial conditions, including highly preordered states, where ions and electrons have been placed on regular lattice structures. In contrast to the ionic plasma component, where such a preordering leads to significant suppression of the heating due to the repulsive ion-ion interactions [92,93], the attractive electron-ion interaction is found to cause electron heating to $\Gamma \lesssim 0.5$ irrespective of the initial state. This clearly excludes the existence of metastable, very strongly coupled two-component plasma states, in which recombination is suppressed by orders of magnitude, as has been suggested recently [63,64] on the basis of numerical simulations.

Nevertheless, the results of the previous sections have shown that the recombination dynamics differs significantly

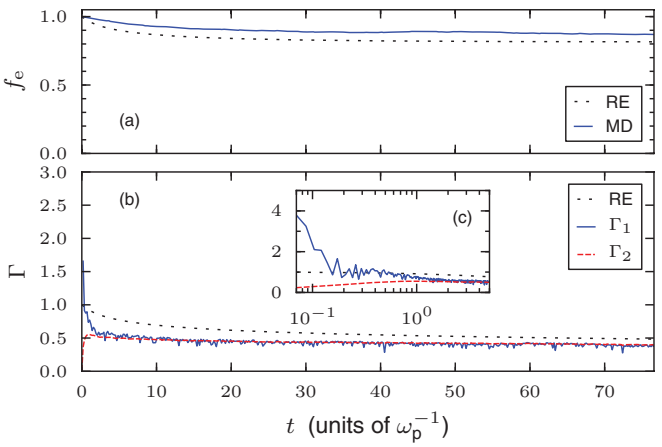

FIG. 9. (Color online) Same as Fig. 8, but for $\Gamma_0 = 1$.

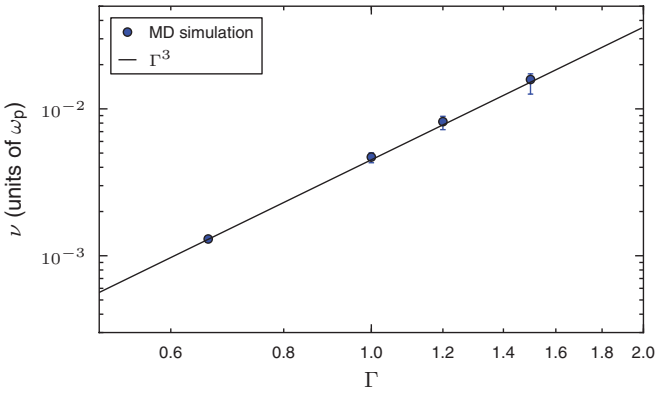

FIG. 10. (Color online) Recombination rate of Fig. 7 (circles) as a function of Γ for intermediate coupling strength. In this range of the coupling parameter the rate scales as Γ^3 (line).

already for $\Gamma \approx 0.5$, yielding a suppression of ν by a factor of 2. Indeed, we observe significant deviations in the time evolution of the free-electron number [see Figs. 8(a) and 9(a)] obtained from the TCP simulations and the rate equations (see Sec. II B). However, in contrast to the OCP results, which solely depend on the actual equilibrium electronic coupling strength Γ, we find an additional dependence of the TCP results on initial electronic excess energy Γ_0: despite the fact that Γ has relaxed to $\sim$0.5 after $\sim 50\,\omega_p^{-1}$ for both $\Gamma_0 = 1$ and $\Gamma_0 = 50$, the number of weakly bound Rydberg atoms differs by about a factor of $\sim$2, which we attribute to the longer relaxation time of the bound states. We anticipate that these effects and deviations from the traditional treatment of recombination may be observable via short-time probing of UCP dynamics.

Indeed, recent measurements of recombination fluorescence on a submicrosecond time scale suggest such deviations [24]. In these experiments, the time-dependent fluorescence from low-lying transitions of recombined atoms has been measured with a time resolution $<$100 ns. At high temperatures, i.e., in the weakly coupled regime, the initial signal $S(t)$ was found to rise proportionally to ρ_e^3, consistent with the picture of isolated three-body collisions, for which $S(t) \sim \rho_e \nu t \propto \rho_e \omega_p \Gamma^{9/2} t \propto \rho_e^3 t$. For lower temperatures, detailed simulations based on three-body CTMC rates predict a density scaling $\sim\rho_e^{1.8}$, while the experiment shows a scaling $\sim\rho_e^{2.2}$. Here it is interesting to note that the recombination rate around $\Gamma \approx 1$ already shows a different scaling $\nu \sim \omega_p \Gamma^3$ (see Fig. 10), giving $\rho_e \nu t \propto \rho_e^{2.5}$. As described in [24], the fluorescence signal is, however, determined also by the initial disorder-induced heating as well as heating due to the formation of Rydberg atoms themselves, such that this simple comparison should be regarded as qualitative only. Nevertheless, MD simulations, as described in this work, combined with a detailed treatment of the radiative cascade of deeply bound states to compare with such measurements may elucidate the role of correlation effects in recombination dynamics of UCPs.

VI. SUMMARY

We have presented extensive numerical simulations of Rydberg-atom formation in plasmas that take into account correlations and many-body interactions between the plasma electrons. This allows us to stretch the focus of such studies deep into the strongly coupled regime, beyond the range of validity of three-body CTMC calculations.

We find quantitative agreement for the recombination rate with previous rate equation calculations [23] in the weakly coupled regime, consistent with a recent study [94]. Such simplified treatments are shown to yield an excellent description, even for Coulomb coupling strengths of up to $\Gamma \approx 0.3$, which covers the typical Γ values obtained in the long-time dynamics of UCPs [11,50].

However, as the electron plasma becomes strongly coupled the bottleneck is found to disappear in the lowered continuum due to increasing electron-electron correlations. In this strongly coupled regime, ν is shown to approach a constant value well below the plasma frequency ω_p, resolving the temperature-divergence problem of the common three-body recombination rate, $\nu \sim T^{-9/2}$, in the ultracold domain.

MD simulations of two component plasmas show that the achievable coupling strength in neutral plasmas is limited to $\Gamma \approx 0.5$, in agreement with recent simulations discussed in [91] while contradicting the findings of [63,64]. Nevertheless, a comparison to the MD results for such coupling parameters suggests that deviations from common rate equation descriptions may be observable in the short-time dynamics of UCPs. We finally note that recent experiments on molecular ultracold plasmas [2,17], realizing much higher densities than atomic systems, show strong deviations from the expansion behavior of atomic systems [10], which, thus far, has been well described within simple rate equation treatment of Rydberg-atom formation [11,15,21]. Exploring the origin of these deviations, however, requires one to account for additional molecular processes [95], which may also alter the plasma expansion behavior.

ACKNOWLEDGMENTS

We thank U. Saalmann and F. Robicheaux for valuable discussions and comments, and are grateful to I. Kabadshow for support with the FMM.

[1] T. C. Killian, S. Kulin, S. D. Bergeson, L. A. Orozco, C. Orzel, and S. L. Rolston, Phys. Rev. Lett. **83**, 4776 (1999).
[2] J. P. Morrison, C. J. Rennick, J. S. Keller, and E. R. Grant, Phys. Rev. Lett. **101**, 205005 (2008).
[3] S. D. Bergeson and R. L. Spencer, Phys. Rev. E **67**, 026414 (2003).
[4] R. S. Fletcher, X. L. Zhang, and S. L. Rolston, Phys. Rev. Lett. **96**, 105003 (2006).
[5] J. T. Mendonca, J. Loureiro, and H. Tercas, J. Plasma Phys. **75**, 713 (2009).
[6] J. Castro, P. McQuillen, and T. C. Killian, Phys. Rev. Lett. **105**, 065004 (2010).

[7] A. Lyubonko, T. Pohl, and J. Rost, e-print arXiv:1011.5937.
[8] J. T. Mendonca and P. K. Shukla, Phys. Plasma **18**, 042101 (2011).
[9] P. K. Shukla, Phys. Lett. A **374**, 3656 (2011).
[10] S. Kulin, T. C. Killian, S. D. Bergeson, and S. L. Rolston, Phys. Rev. Lett. **85**, 318 (2000).
[11] F. Robicheaux and J. D. Hanson, Phys. Rev. Lett. **88**, 055002 (2002).
[12] F. Robicheaux and J. D. Hanson, Phys. Plasma **10**, 2217 (2003).
[13] T. Pohl, T. Pattard, and J. M. Rost, Phys. Rev. A **68**, 010703 (2003).
[14] T. Pohl, T. Pattard, and J. M. Rost, Phys. Rev. A **70**, 033416 (2004).
[15] S. Laha, P. Gupta, C. E. Simien, H. Gao, J. Castro, T. Pohl, and T. C. Killian, Phys. Rev. Lett. **99**, 155001 (2007).
[16] K. A. Twedt and S. L. Rolston, Phys. Plasma **17**, 082101 (2010).
[17] J. P. Morrison, C. J. Rennick, and E. R. Grant, Phys. Rev. A **79**, 062706 (2009).
[18] X. L. Zhang, R. S. Fletcher, and S. L. Rolston, Phys. Rev. Lett. **101**, 195002 (2008).
[19] M. Rosenberg and P. K. Shukla, Phys. Scr. **83**, 015503 (2011).
[20] T. C. Killian, M. J. Lim, S. Kulin, R. Dumke, S. D. Bergeson, and S. L. Rolston, Phys. Rev. Lett. **86**, 3759 (2001).
[21] P. Gupta, S. Laha, C. E. Simien, H. Gao, J. Castro, T. C. Killian, and T. Pohl, Phys. Rev. Lett. **99**, 075005 (2007).
[22] R. S. Fletcher, X. L. Zhang, and S. L. Rolston, Phys. Rev. Lett. **99**, 145001 (2007).
[23] T. Pohl, D. Vrinceanu, and H. R. Sadeghpour, Phys. Rev. Lett. **100**, 223201 (2008).
[24] S. D. Bergeson and F. Robicheaux, Phys. Rev. Lett. **101**, 073202 (2008).
[25] T. Killian, T. Pattard, T. Pohl, and J. Rost, Phys. Rep. **449**, 77 (2007).
[26] T. C. Killian, Science **316**, 705 (2007).
[27] T. C. Killian and S. L. Rolston, Phys. Today **63**, 46 (2010).
[28] B. J. Claessens, S. B. van der Geer, E. J. D. Vredenbregt, and O. J. Luiten, Phys. Rev. Lett. **95**, 164801 (2005).
[29] J. L. Hanssen, J. J. McClelland, E. A. Dakin, and M. Jacka, Phys. Rev. A **74**, 063416 (2006).
[30] M. P. Reijnders, P. A. van Kruisbergen, G. Taban, S. B. van der Geer, P. H. A. Mutsaers, E. J. D. Vredenbregt, and O. J. Luiten, Phys. Rev. Lett. **102**, 034802 (2009).
[31] A. J. McCulloch, D. V. Sheludko, S. D. Saliba, S. C. Bell, M. Junker, K. A. Nugent, and R. E. Scholten, Nat. Phys. **7**, 785 (2011).
[32] S. Ichimaru, Rev. Mod. Phys. **54**, 1017 (1982).
[33] R. Redmer, Phys. Rep. **282**, 35 (1997).
[34] D. H. E. Dubin and T. M. O'Neil, Rev. Mod. Phys. **71**, 87 (1999).
[35] M. Bonitz, C. Henning, and D. Block, Rep. Prog. Phys. **73**, 066501 (2010).
[36] M. S. Murillo, Phys. Rev. Lett. **87**, 115003 (2001).
[37] S. Mazevet, L. A. Collins, and J. D. Kress, Phys. Rev. Lett. **88**, 055001 (2002).
[38] S. G. Kuzmin and T. M. O'Neil, Phys. Rev. Lett. **88**, 065003 (2002).
[39] C. E. Simien, Y. C. Chen, P. Gupta, S. Laha, Y. N. Martinez, P. G. Mickelson, S. B. Nagel, and T. C. Killian, Phys. Rev. Lett. **92**, 143001 (2004).
[40] E. A. Cummings, J. E. Daily, D. S. Durfee, and S. D. Bergeson, Phys. Rev. Lett. **95**, 235001 (2005).
[41] S. D. Bergeson, A. Denning, M. Lyon, and F. Robicheaux, Phys. Rev. A **83**, 023409 (2011).
[42] G. Zwicknagel, Contrib. Plasma Phys. **39**, 155 (1999).
[43] Y. C. Chen, C. E. Simien, S. Laha, P. Gupta, Y. N. Martinez, P. G. Mickelson, S. B. Nagel, and T. C. Killian, Phys. Rev. Lett. **93**, 265003 (2004).
[44] T. Pohl, T. Pattard, and J. M. Rost, Phys. Rev. Lett. **94**, 205003 (2005).
[45] P. K. Shukla and K. Avinash, Phys. Rev. Lett. **107**, 135002 (2011).
[46] T. Pohl, T. Pattard, and J. M. Rost, Phys. Rev. Lett. **92**, 155003 (2004).
[47] M. Bonitz, V. S. Filinov, V. E. Fortov, P. R. Levashov, and H. Fehske, Phys. Rev. Lett. **95**, 235006 (2005).
[48] H. Kählert and M. Bonitz, Phys. Rev. Lett. **104**, 015001 (2010).
[49] P. Mansbach and J. Keck, Phys. Rev. **181**, 275 (1969).
[50] R. S. Fletcher, X. L. Zhang, and S. L. Rolston, Phys. Rev. Lett. **99**, 145001 (2007).
[51] J. Stevefelt, J. Boulmer, and J. F. Delpech, Phys. Rev. A **12**, 1246 (1975).
[52] L. Vriens and A. H. M. Smeets, Phys. Rev. A **22**, 940 (1980).
[53] B. Zygelman, J. Phys. B **38**, S387 (2005).
[54] E. Hinnov and J. G. Hirschberg, Phys. Rev. **125**, 795 (1962).
[55] M. Schlanges and T. Bornath, Physica A **192**, 262 (1993).
[56] M. Schlanges and T. Bornath, Physica A **196**, 427 (1993).
[57] D. Kremp, M. Schlanges, M. Bonitz, and T. Bornath, Phys. Fluids B **5**, 216 (1993).
[58] T. Bornath, T. Ohde, and M. Schlanges, Physica A **211**, 344 (1994).
[59] D. Kremp, T. Bornath, M. Bonitz, W. D. Kraeft, and M. Schlanges, Phys. Plasma **7**, 59 (2000).
[60] Y. Hahn, Phys. Lett. A **231**, 82 (1997).
[61] Y. Hahn, Phys. Rev. E **64**, 046409 (2001).
[62] B. Zygelman, J. Phys. B **36**, L31 (2003).
[63] A. V. Lankin and G. E. Norman, J. Phys. A **42**, 214042 (2009).
[64] A. A. Bobrov, S. Y. Bronin, B. B. Zelener, B. V. Zelener, E. A. Manykin, and D. R. Khikhlukha, J. Exp. Theor. Phys. **112**, 527 (2011).
[65] S. G. Kuzmin and T. M. O'Neil, Phys. Plasma **9**, 3743 (2002).
[66] M. Amoretti *et al.*, Nature **419**, 456 (2002).
[67] G. Gabrielse *et al.*, Phys. Rev. Lett. **89**, 213401 (2002).
[68] G. Gabrielse, Adv. At. Mol. Opt. Phys. **50**, 155 (2005).
[69] M. Glinsky and T. M. O'Neil, Phys. Fluids B **3**, 1270 (1991).
[70] F. Robicheaux and J. D. Hanson, Phys. Rev. A **69**, 010701 (2004).
[71] T. Pohl, H. R. Sadeghpour, and G. Gabrielse, Phys. Rev. Lett. **97**, 143401 (2006).
[72] E. M. Bass and D. H. E. Dubin, Phys. Plasma **3**, 012101 (2009).
[73] F. Robicheaux, J. Phys. B **41**, 192001 (2008).
[74] T. Pohl, H. R. Sadeghpour, and P. Schmelcher, Phys. Rep. **484**, 181 (2009).
[75] L. Greengard and V. Rokhlin, J. Comput. Phys. **73**, 325 (1987).
[76] C. G. Lambert, T. A. Darden, and J. A. B. Jr., J. Comput. Phys. **126**, 274 (1996).
[77] H. Dachsel, J. Chem. Phys. **132**, 119901 (2010).
[78] H. Dachsel and I. Kabadshow, see [www2.fz-juelich.de/jsc/fmm]
[79] P. P. Ewald, Ann. Phys. (NY) **369**, 253 (1921).

[80] A. Y. Toukmaji and J. A. Board, Comput. Phys. Commun. **95**, 73 (1996).
[81] M. Tuckerman, B. J. Berne, and G. J. Martyna, J. Chem. Phys. **97**, 1990 (1992).
[82] S. J. Stuart, R. Zhou, and B. J. Berne, J. Chem. Phys. **105**, 1426 (1996).
[83] S. G. Brush, H. L. Sahlin, and E. Teller, J. Chem. Phys. **45**, 2102 (1966).
[84] J. P. Hansen, Phys. Rev. A **8**, 3096 (1973).
[85] W. L. Slattery, G. D. Doolen, and H. E. DeWitt, Phys. Rev. A **21**, 2087 (1980).
[86] M. S. Murillo and J. C. Weisheit, Phys. Rep. **302**, 1 (1998).
[87] Z. Donkó, G. J. Kalman, and K. I. Golden, Phys. Rev. Lett. **88**, 225001 (2002).
[88] I. Georgescu, U. Saalmann, and J. M. Rost, Phys. Rev. A **76**, 043203 (2007).
[89] D. R. Bates, A. E. Kingston, and R. W. P. McWhirter, Proc. R. Soc. London A **267**, 297 (1962).
[90] A. Burgess and H. Summers, Mon. Not. R. Astron. Soc. **174**, 345 (1976).
[91] K. Niffenegger, K. A. Gilmore, and F. Robicheaux, J. Phys. B **44**, 145701 (2011).
[92] D. Gericke and M. Murillo, Contrib. Plasma Phys. **43**, 298 (2003).
[93] T. Pohl, T. Pattard, and J. M. Rost, J. Phys. B **37**, L183 (2004).
[94] J. P. Morrison, N. Saquet, and E. R. Grant (to be published in J. Phys. B).
[95] N. Saquet, J. P. Morrison, M. Schulz-Weiling, H. Sadeghi, J. Yiu, C. J. Rennick, and E. R. Grant, J. Phys. B **44**, 184015 (2011).